DOE/ET-53088-347 IFSR #347

Particle Simulation of Toroidicity-Induced Drift Modes

M.J. LeBrun and *T. Tajima*
Department of Physics and
Institute for Fusion Studies
The University of Texas at Austin
Austin, Texas 78712

October 1988

Particle Simulation of Toroidicity-Induced Drift Modes

M.J. LeBrun and T. Tajima
Department of Physics and Institute for Fusion Studies,
University of Texas at Austin
Austin,TX 78712

The linear and nonlinear behavior of the toroidicity induced drift mode is studied using a three dimensional, natural coordinate electrostatic particle code. In this simulation an instability involving radially extended toroidal drift modes, showing a banded frequency structure, is observed for the first time. Nonlinear phenomena such as the enhancement of instability by toroidal mode multiplicity, saturation, and particle transport are also reported.

PACS numbers : 52.65.+z

The drift or universal instability has long been suspected to play a strong role in the anomalous transport observed in plasma experiments. It has attracted much theoretical attention because of its ubiquitous nature, being driven by a density gradient alone, and is known to be absolutely stable within the confines of the sheared slab model [1,2,3]. However, toroidal effects fundamentally alter the behavior of the drift mode [4,5]. In this system, the drift wave eigenmodes at neighboring mode rational surfaces become strongly coupled, annihilating the ion shear damping. This results in the radially extended, toroidicity-induced (TI) drift instability [6].

In this Letter, we report on the first self-consistent electrostatic particle simulations of a tokamak-like plasma in the TI-mode regime. Previous related efforts include the study of the trapped particle instability by Cheng and Okuda [7], and the study of the of the nonlinear destabilization of the slab drift wave by Sydora *et al* [8]. The work of Cheng and Okuda [7,9] demonstrated the feasability of large scale three-dimensional particle simulation in a non-Cartesian metric, and the development of large core memory machines (e.g. Cray-2) has made such methods increasingly practical. The algorithm we have developed utilizes an orthogonal flux coordinate system in a nearly arbitrary metric and is much better suited for the study of radially localized modes such as drift waves (details of this method will be reported elsewhere [10]).

In the present simulation model, the entire plasma profile is represented

by the particle species. Field quantities are represented on a two-dimensional grid in (r, θ) and a mode expansion in ϕ; a nonuniform radial grid generation method [10] is employed to increase radial resolution near the mode rational surfaces. An iterative method of solving the toroidal Poisson equation is used. Ion dynamics are modeled exactly, while electrons follow drift-type dynamics given by the equations of motion $\mathbf{v}_d = \mathbf{u}_e + (\mathbf{b}/\Omega_e) \times \left\{ (\mu/m) \nabla B + v_{\|}^2 (\mathbf{b} \cdot \nabla \mathbf{b}) \right\}$ and $dv_{\|}/dt = -(e/m) E_{\|} - (\mu/m) \mathbf{b} \cdot \nabla B$, where $\mathbf{u}_e = \mathbf{E} \times \mathbf{b}/B$, $\mathbf{b} = \mathbf{B}/B$, $\mu = \frac{1}{2} m v_{\perp}^2 / B$, $\Omega_e = eB/mc$, and m is the electron mass.

Simulation runs employing a single "high" toroidal mode number $n = 9$ were performed for two values of $k_{\perp} \rho_s$ (0.2 and 0.4) and inverse aspect ratio of $a/R_0 = 0.4$; these runs were repeated in the cylindrical limit of the code as a control case. The mode rational surfaces contained within the system ranged from $q \sim 0.56$ ($m = 5$) to $q \sim 1.67$ ($m = 15$). "Undesired" mode rational surfaces (for which the eigenmodes are not confined within the system) are excluded by eliminating the appropriate Fourier components of the electric potential. The drift ion resonance layers are contained within the simulation region for each mode rational surface thus selected. An additional set of runs including a multiplicity of toroidal harmonics were carried out to study the enhancement of growth rate and saturation level due to the stochastic-electron mechanism of Hirshman and Molvig [11]. The initial velocity distributions are Maxwellian, with $T_e = T_i$, $T_{\|}/T_{\perp} = 2$, and $v_e = 1.56 \, \Delta_0 \, \omega_e^{-1}$ (ω_e is the plasma frequency). The remaining simulation

parameters are given by : $N_p = 98304$ (number of particles), $N_r = N_\theta = 128$, $\Delta t = 4.0\,\omega_e^{-1}$, $m_e/m_i = 0.01$, $\Omega_e/\omega_e = 10$, and particle "size" approximately one grid spacing in both the radial and poloidal coordinates (using two passes of a binomial digital filter for the radial grid). The gaussian density profile is given by $n(r) \sim n_0 \exp\left[-(\kappa_0 r)^2/2\right]$ with $\kappa_0\, a = 4.8$, and $a = 128\Delta_0$ the minor radius ($\kappa_0 \rho_s \simeq 0.041$). We then have $\omega^*/\Omega_i = (\kappa\rho_s)(k_\perp\rho_s) = m(\kappa_0\rho_s)^2$, where $\kappa = L_n^{-1} = \partial \ln n/\partial r$, so that the only variation of the electron diamagnetic frequency ω^* is through the poloidal mode number m. We will devote the bulk of our presentation on the results of the $k_\perp\rho_s \sim 0.2$ cylindrical (control) and toroidal runs. For these cases, the value of $k_\perp\rho_s$ evaluated at the mode rational surfaces varies only weakly, having a minimum value of 0.165 for $m = 6$ and a maximum of 0.219 for $m = 15$.

For theoretical corroboration with the simulation results, we shall compare to the work of Schep and Venema [12]. Parameters in the central region are comparable to those used in the theoretical calculation [12], for which $\epsilon_n \sim 0.1$ ($\equiv L_n/R_0$) and $\hat{s}(\equiv rq'/q) \sim 1$. The simulation employs $k_\perp\rho_i \sim 0.2$, for which the growth rate of the TI-mode is expected to be a maximum. Compromises due to computational and/or algorithmic limitations include the relatively large inverse aspect ratio in the simulation (roughly twice that of the theoretical work), and large electron/ion mass ratio. In addition, in the simulation most quantities (shear, diamagnetic frequency) vary significantly over the radial extent, while the theoretical treatment assumes the

only radial variation is through the variation in the safety factor $q(r)$.

The simulations for a single toroidal harmonic $n = 9$ with $k_\perp \rho_s \sim 0.2$ are run for a total of 15,000 time-steps ($t = 6000\,\Omega_i^{-1}$). For the toroidal run, modification of the electron density profile is observed until about $t = 1200\,\Omega_i^{-1}$. In Figure 1 (a) we plot the electron density profile initially and at time $t = 1200\,\Omega_i^{-1}$. Also shown in Figure 1 is the location of the mode rational surfaces and radial grid spacing and the radial variation of the safety factor, q.

An obvious feature is a definite profile modification about the $m = 5$ mode rational surface, which is highly localized. This occurs in both the cylindrical and toroidal runs, and is therefore not a toroidal effect. Further, the growth rate of the potential at this location is much larger than that expected for a drift mode. Since the curvature at the $m = 5$ mode rational surface is quite strong, a gravitational-type instability may be responsible for the observed behavior there.

Additional profile modification occurs from about the $m = 7$ to the $m = 10$ mode rational surfaces in the toroidal case, but not in the cylindrical case. The potential for these modes is found to grow exponentially until roughly $t = 1000\,\Omega_i^{-1}$, at which time significant profile modification ceases as well. The time evolution of $|e\Phi/T|$ is shown in Figure 2 (a) for the $m = 8$ mode for a typical radial position near the mode rational surface. The growth rate is measured to be approximately $\gamma/\Omega_i \sim 1.25 \times 10^{-3}$, or $\gamma/\omega^* \sim 0.075$ (note

$\Omega_i/\omega^* \sim 60.0$). The measured value is roughly a factor of three larger than the value predicted theoretically [12], which may be due in part to the trapped electrons present in the simulation (neglected in the theory) and to the rough association of parameters between the theory and simulation (the increase in both the inverse aspect ratio and mass ratio is expected to be destabilizing [12]). Saturation for these modes occurs at a level of $|e\Phi/T| \sim 0.04$ (for reference our $\rho_s/L_n \sim 0.075$). The toroidal run with $k_\perp \rho_s \sim 0.4$ showed growth for the $m = 8$ mode as well, with the growth rate observed to be $\gamma/\omega^* \sim 0.057$. No growth in the potential for this mode and radial position was observed in the cylindrical runs, leaving the observed toroidal behavior as strong evidence of the toroidicity-induced mode.

A run employing toroidal mode numbers $n = 7$ through $n = 11$ was undertaken, with otherwise the same parameters as the single-n case. Growth of the potential was observed for a number of (m, n) pairs, with growth rates as large as a factor of two greater than in the single n run. The time evolution of $|e\Phi/T|$ for the $m = 8$, $n = 10$ mode from this run is plotted in Figure 2 (b), showing a saturation value of $|e\Phi/T| \sim 0.06$ and growth rate of $\gamma/\omega^* \sim 0.132$.

We examine the mode structure of the potential on long time scales via spectral analysis for the toroidal single-n run. The power spectrum is calculated by the maximum entropy method; peaks in the calculated spectrum are located numerically for each radial position and mode number, with only the strongest power peaks retained. The observed frequency spectrum, as

a function of radius and mode number, has many new noteworthy features. First, we see a multiplicity of modes with frequencies below the diamagnetic frequency. This result is a consequence of the strong coupling of the poloidal modes in toroidal geometry, which allows multiple toroidal drift harmonics to appear. In Figure 3 (a) & (b) where we have plotted the observed wave frequency ω as a function of radius, and power versus ω, both for the $m = 7$ mode. In these plots, each mark denotes the presence of a signal, and some of the lowest power signals have been removed. Note that the ion magnetic drift frequency is on the order of $\bar{\omega}_{D_i}/\Omega_i \sim 0.001$, so the ion magnetic drift resonance may significantly affect the lowest harmonic. The modes are seen to propagate in the direction of the electron diamagnetic drift.

Comparing the frequency dependence on the radius for neighboring mode numbers, we see a dramatic preference for certain frequency bands (which may vary with position), especially at low frequency. This is demonstrated in Figure 3 (c), in which the response for the $m = 7$ through $m = 11$ modes is plotted. The lowest two frequency bands show the highest degree of overlap, and are by far the strongest modes. The frequency of the lowest harmonic is given roughly by $\omega/\omega^* \sim 0.26$, and the second harmonic by $\omega/\omega^* \sim 0.55$, compared to the (single) theoretical value [12] of $\omega/\omega^* \sim 0.4$. The cylindrical run, on the other hand, shows no band structure in its frequency response, as expected. In addition, the lowest harmonic seen in the cylindrical run has a frequency approximately that of the second harmonic in the toroidal run;

the ultra-low frequency harmonic appears only in the toroidal case.

Most modes extend over a large number of mode rational surfaces, but still show some radial localization. This is consistent with the physics of the parameter regime. The mode coupling in this case is reduced by the variation of the diamagnetic frequency with radius, which differs by a factor of three between the highest and lowest mode numbers, and by the radial variation of the shear. Thus the mode structure cannot be completely described by either the strong coupling (ballooning mode) or weak coupling (Fourier mode) limits, but a mix of aspects of each. Qualitatively, the variation of ω^* with radius will reduce the number of poloidal modes involved in a single quasimode, and limit the radial extent. The changing ω^* is expected to give a radial variation to the resulting frequency spectrum, which is observed in the simulation results via an upward trend in frequency with increasing radial position.

The radial structure via the interferogram diagnostic [13] shows peaking of the potential near the mode rational surface for the observed frequencies. The waveforms are typically highly oscillatory in r and overlap an appreciable number of adjacent mode rational surfaces. This behavior is a consequence of the weakly damped or unstable, radially extended character of the mode, in contrast to the rapid radial decay of the slab geometry drift mode eigenfunction. Radial interferograms for the $m = 12$ mode are shown in Figure 4 (a) & (b) for the toroidal and cylindrical runs. The width of the interfered po-

tential in the toroidal case is approximately twice that in the cylindrical run, demonstrating the radially-extended nature of the toroidal mode. Note that the finite radial width of the TI-mode eigenfunction is caused by the variation of equilibrium quantities with r (such as the diamagnetic frequency), and from our truncation of the poloidal mode space.

The interferogram in the poloidal angle shows another aspect of the toroidal nature of these modes. Theoretically, strongly coupled modes exhibit "ballooning" towards the outside of the torus. This ballooning behavior is observed in the simulation, for several frequency ranges and at many radial grid points; a representative interferogram is displayed in Figure 4 (c). For the case shown, the maximum amplitude occurs away from the $\theta = 0$ axis (outward direction), although more usually the maximum occurs on the axis.

The particle diffusion which occurs as a result of these unstable modes can be obtained through the use of test particles [8]. In the course of each run, 100 test particles are followed in time. These are initially uniformly distributed in the region of interest. The diffusion coefficient calculated from this diagnostic was observed to be $D \sim 1.4\rho_s^2\omega^*$ for the multiple-n toroidal run, $D \sim 0.60\rho_s^2\omega^*$ for the single-n toroidal run, and $D \sim 0.36\rho_s^2\omega^*$ for the cylindrical (control) run. With the diffusion coefficient $D = (\delta r^2/t_{cor})$ where $(\delta r/\rho_s) \sim (e\Phi/T)(k_\perp\rho_s)(t_{cor}\Omega_i)$, and using the observed value of the saturation level of Φ, we obtain the correlation time of turbulence as $\omega^* t_{cor} \sim 2.2$ for the multiple-n and single-n cases.

This work was supported by the U. S. Department of Energy under Contract No. DE-FG05-80ET53088 and by the National Science Foundation under Grant No. ATM 88-11128.

References

[1] N. A. Krall and M. N. Rosenbluth, Phys. Fluids **8**, 1488 (1965).

[2] D. W. Ross and S. M. Mahajan, Phys. Rev. Lett. **40**, 324 (1978).

[3] K. T. Tsang, P. J. Catto, J. C. Whitson, and J. Smith, Phys. Rev. Lett. **40**, 327 (1978).

[4] J. B. Taylor, in *Plasma Physics and Controlled Nuclear Fusion Research*, p. 323 (1977).

[5] W. Horton, R. Estes, H. Kwak, and D. Choi, Phys. Fluids **21**, 1366 (1978).

[6] L. Chen and C. Z. Cheng, Phys. Fluids **23**, 2242 (1980).

[7] C. Z. Cheng and H. Okuda, Phys. Rev. Lett. **41**, 1116 (1978).

[8] R. D. Sydora, J. N. Leboeuf, D. R. Thayer, P. H. Diamond, and T. Tajima, Phys. Rev. Lett. **57**, 3269 (1986).

[9] C. Z. Cheng and H. Okuda, J. Comp. Phys. **25**, 133 (1977).

[10] M. J. LeBrun and T. Tajima, to be published.

[11] S. P. Hirshman and K. Molvig, Phys. Rev. Lett. **42**, 648 (1979).

[12] T. J. Schep and M. Venema, Plasma Physics and Controlled Fusion **27**, 653 (1985).

[13] V. K. Decyk, J. M. Dawson, and G. J. Morales, Phys. Fluids **22**, 507 (1979).

1 Figure Captions

1. (a) Electron density profiles at time $t = 0$ (solid line), and time $t = 1200\,\Omega_i^{-1}$ (dashed line). (b) Positions of mode rational surfaces ($q = 5/9$ to $15/9$) and radial grid spacing. (c) Safety factor q as a function of r.

2. (a) $|e\Phi/T|$ versus time for the $m = 8$ mode, toroidal single-n run, at a radial position near the mode rational surface. (b) $|e\Phi/T|$ versus time for the $m = 8, n = 10$ mode in the toroidal multiple-n run.

3. Frequencies and power spectrum obtained from spectral analyzer: (a) Power as a function of ω/Ω_i for the $m = 7$ mode. (b) ω/Ω_i as a function of radius for the $m = 7$ mode. (c) ω/Ω_i as a function of radius for the $m = 7$ through $m = 11$ modes. The arrows mark the location of the mode rational surfaces ($q = m/n = 7/9$ through $11/9$).

4. (a) & (b) Interferograms of the potential for the toroidal run and cylindrical run, respectively. These are plotted versus r for the $m = 12$ mode, both real part (solid line) and imaginary (dotted line). (c) Amplitude interferogram of the potential plotted versus θ for a given value of r.

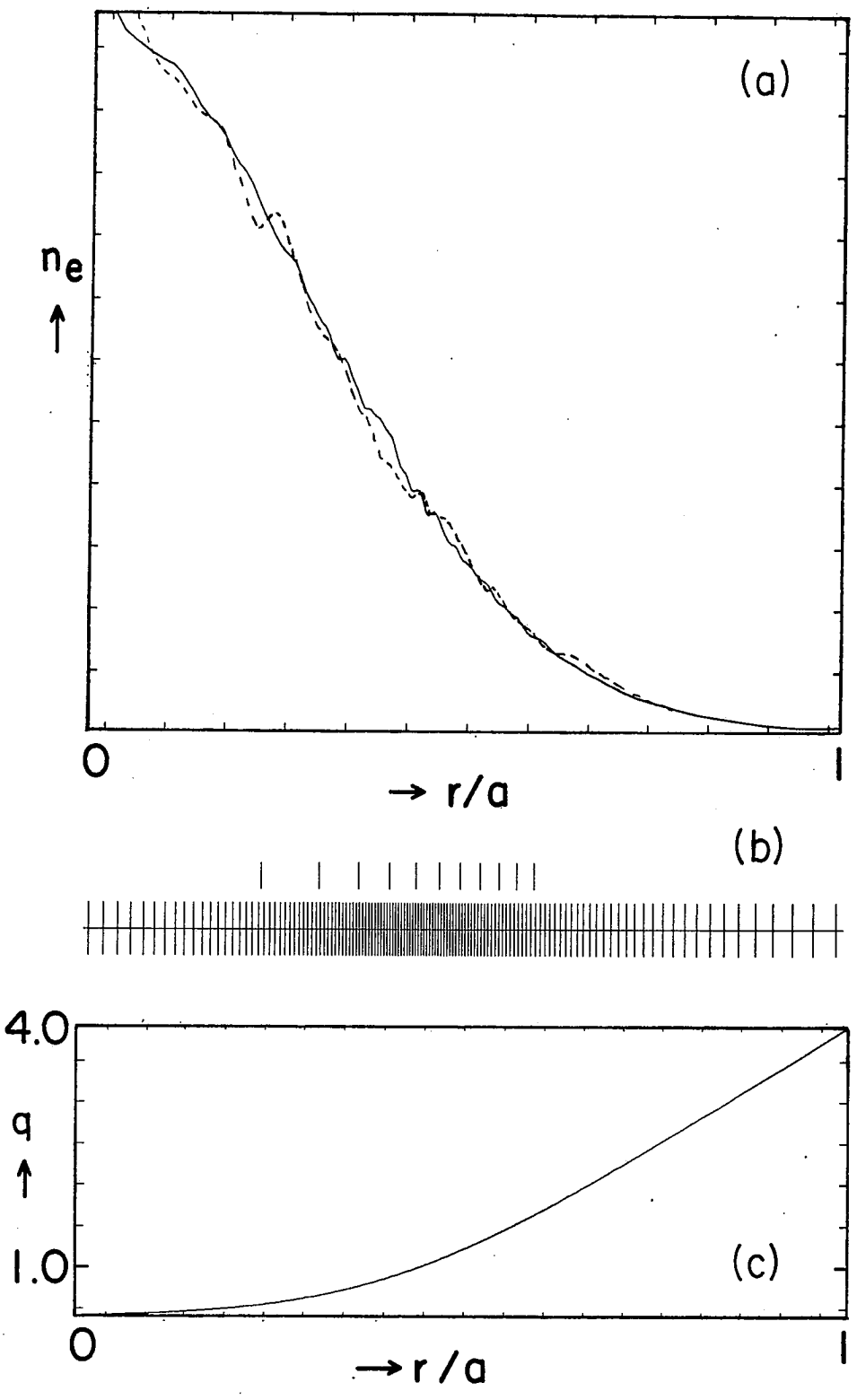

Figure 1

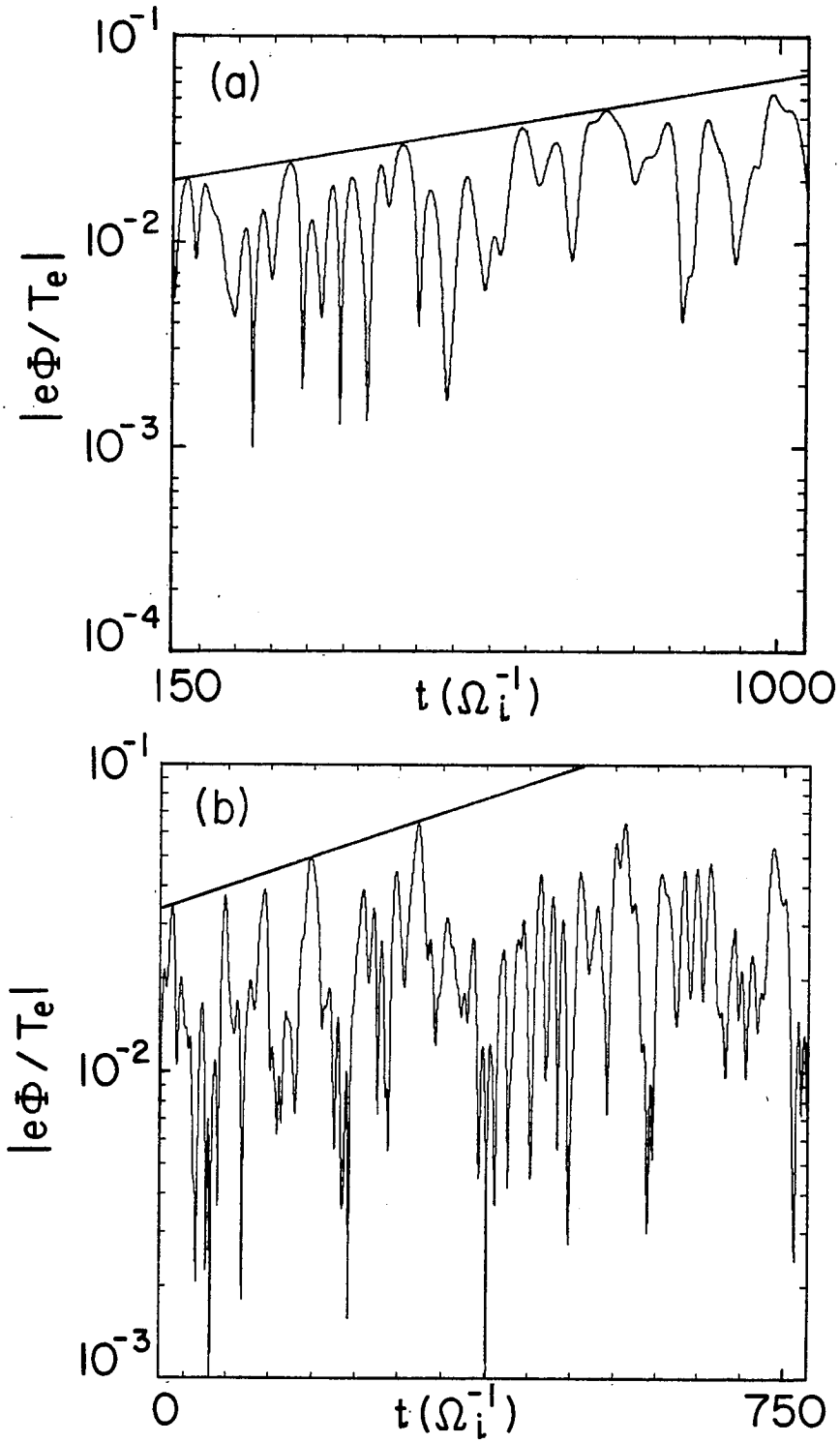
(a)
10^{-1}
10^{-2}
10^{-3}
10^{-4}
$|e\Phi/T_e|$
150
$t(\Omega_i^{-1})$
1000
(b)
10^{-1}
10^{-2}
10^{-3}
$|e\Phi/T_e|$
0
$t(\Omega_i^{-1})$
750

Figure 2

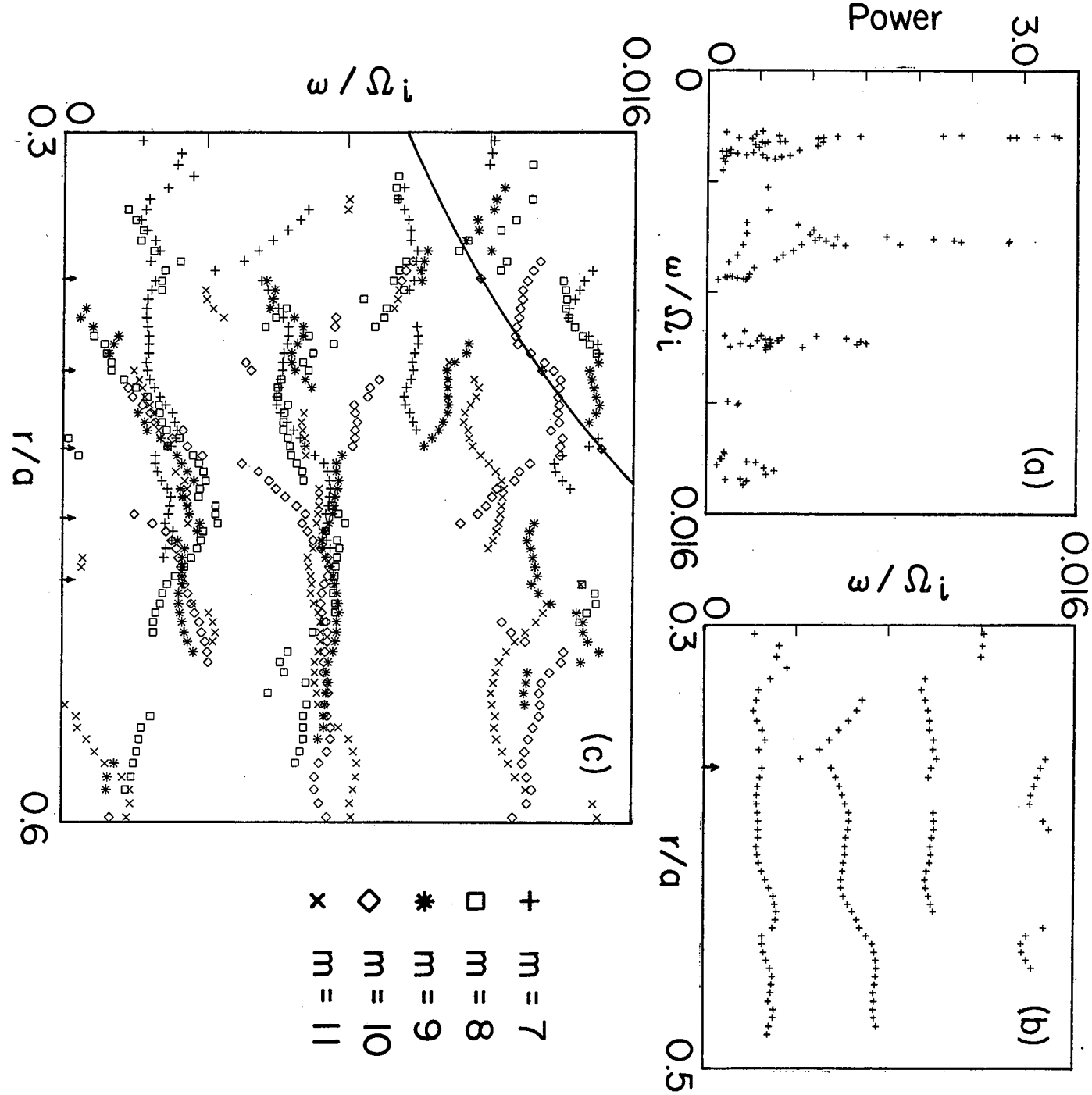
Power
3.0
0
0
ω / Ω_i
0.016
(a)
0.016
ω / Ω_i
0
0.3
r/a
0.5
(b)
ω / Ω_i
0
0.016
0.3
r/a
0.6
(c)
m = 7
m = 8
m = 9
m = 10
m = 11

Figure 3

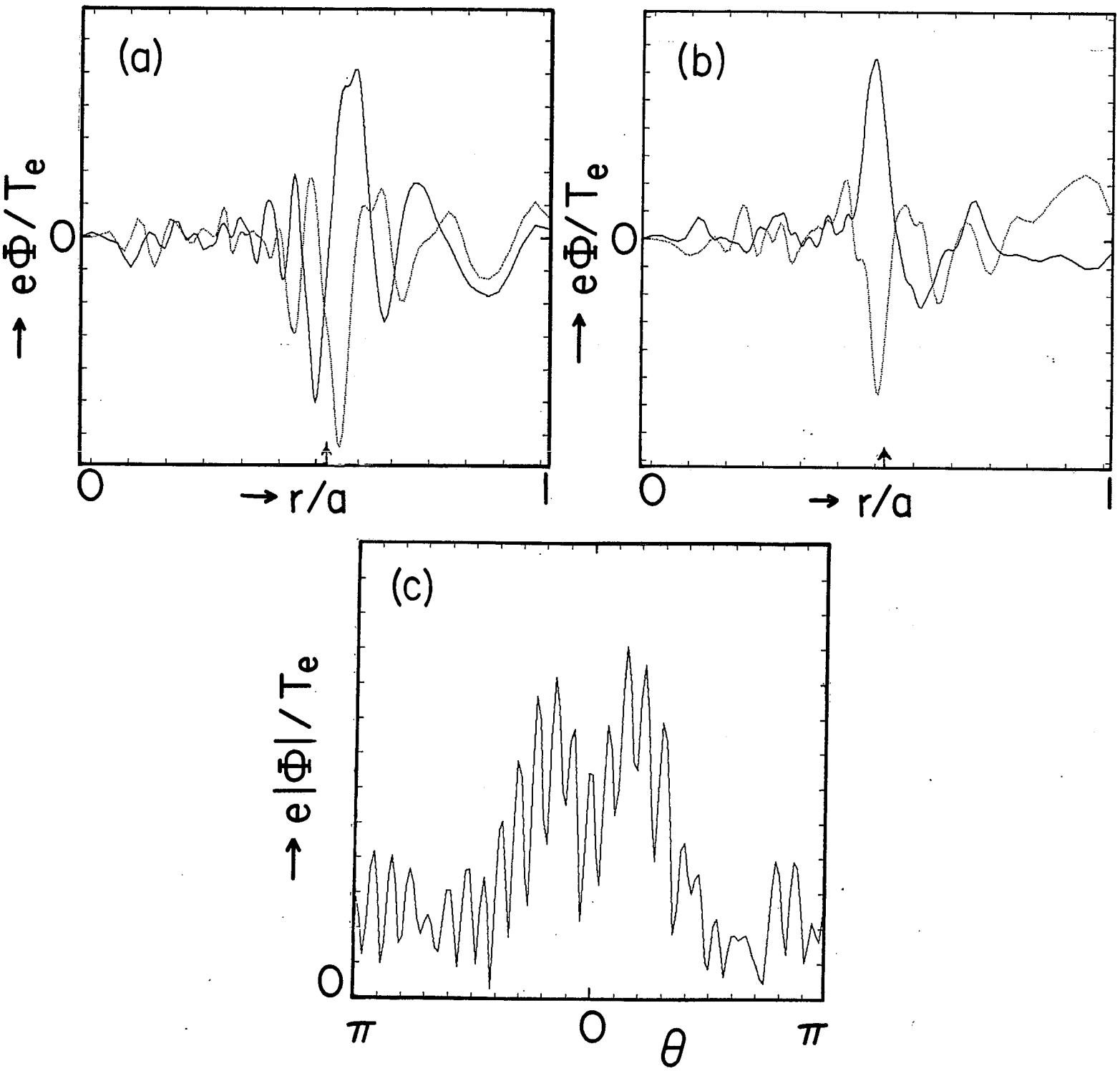

Figure 4